Available online at www.sciencedirect.com

jmr&t Journal of Materials Research and Technology

journal homepage: www.elsevier.com/locate/jmrt

Original Article

Coupled role of alloying and manufacturing on deep cryogenic treatment performance on high-alloyed ferrous alloys

Patricia Jovičević-Klug [a,b,*], *Agnieszka Zuzanna Guštin* [a], *Matic Jovičević-Klug* [a,c], *Barbara Šetina Batič* [a], *Andrej Lebar* [d,e], *Bojan Podgornik* [a,b]

[a] *Institute of Metals and Technology, Lepi Pot 11, 1000 Ljubljana, Slovenia*
[b] *Jožef Stefan International Postgraduate School, Jamova Cesta 39, 1000 Ljubljana, Slovenia*
[c] *Max Planck Institute for Iron Research, Max-Planck-Straße 1, 40237 Düsseldorf, Germany*
[d] *University of Ljubljana, Faculty of Mechanical Engineering, Aškrčeva Ulica 6, 1000 Ljubljana, Slovenia*
[e] *University of Ljubljana, Faculty of Health Sciences, Zdravstvena Pot 5, 1000 Ljubljana, Slovenia*

ARTICLE INFO

Article history:
Received 25 January 2022
Accepted 3 April 2022
Available online 8 April 2022

Keywords:
Deep cryogenic treatment
Alloying content
Manufacturing type
Ferrous alloy
Carbides precipitation
Mechanical properties

ABSTRACT

This study focuses on influence of alloying content and type of manufacturing on the effectiveness of deep cryogenic treatment (DCT) on properties of selected high-alloyed ferrous alloys (HAFA): EN HS6-5-2, EN HS6-5-2-5, EN HS6-5-3 and EN HS12-1-4. In order to evaluate the dependency of DCT performance on chemical composition and manufacturing type, the microstructure, hardness, impact and fracture toughness and fatigue properties were analyzed. Additionally, the fatigue data was evaluated using an adapted strain-life model in order to understand the unique effects of DCT with selected factors and provide a model for estimating the fatigue limit of DCT HAFA. The study indicates that DCT affects carbide precipitation, size and morphology of nanocarbides, average distance between carbides and nanocarbides, as well as the base matrix (martensitic laths). The induced microstructural changes cause an overall positive change of mechanical properties in selected HAFA, which correlates well with individual alloying and manufacturing differences. Overall, DCT has greater effect on wrought HAFA than powder metallurgy manufactured HAFA, at which high content of W and Co generally degenerates the DCT induced microstructure modifications.

1. Introduction

Chemistry and manufacturing procedure of ferrous alloys are important factors, which influence the microstructure development and consequentially final properties of ferrous alloys [1]. In the case of high-alloyed ferrous alloys (HAFA), the alloy is heavily loaded with alloying elements (Cr, V, W, Ni, Ti, Co and Mo), which allow development of superior combinations of mechanical, fatigue, corrosive and wear properties of

* Corresponding author.
E-mail address: patricia.jovicevicklug@imt.si (P. Jovičević-Klug).
https://doi.org/10.1016/j.jmrt.2022.04.025

the alloy for selected applications in comparison to low-alloyed ferrous alloys [1]. Cr is added in order to increase resistance to oxidation/corrosion and hardenability of steel, Ni increases the corrosion resistance and toughness, Mo improves strength, V prevents grain coarsening during the heat treatment and improves strength, Co improves heat resistance and retards grain coarsening, while W improves hardness and resistance to wear, cutting and heat resistance [1]. The chemical composition influences the development of the matrix (austenite, ferrite, martensite and pearlite) and the volume fraction of carbide precipitation (MC, M_6C and $M_{23}C_6$) [1]. Another important factor, which influences the performance of HAFA, is the type of manufacturing (type of production scheme), which can be roughly divided into wrought production - and powder metallurgy (PM) [1]. For wrought ferrous alloys the manufacturing is conducted usually in a 2-step process, at which firstly the ferrous alloy is melted and produced in ingots through casting or continuous casting processes and in the second step the ingots are reheated and hot rolled to final dimensions [1]. For PM manufacturing the ferrous alloy is made from metallic powders in 3 steps: powder blending, die compaction and final sintering [1]. For both production types the final products are usually finally heat treated with soft annealing to soften the alloy for machining purposes. Due to the different manufacturing type of PM and wrought ferrous alloys, the process selection consequently influences the microstructure (distribution, precipitation, size and morphology) and thus the hardenability, porosity and other properties of ferrous alloys [1].

In addition to chemical composition and type of manufacturing of HAFA, the proper selection of heat treatment is an additional factor, which consequently influences the final microstructure and properties of HAFA [1]. Traditional heat treatment of HAFA consists of heating to the austenitization temperature, quenching in water, oil or with high pressure gas and multiple tempering. However, traditional heat treatment can also be combined with deep cryogenic treatment (DCT), where the ferrous alloy is exposed to temperatures below −160 °C, usually to liquified nitrogen, in order to induce the change of retained austenite (RA) into martensite, induce precipitation of additional carbides and to modify their distribution and size [2]. There have been some studies conducted in relation to HAFA treated with DCT [3–9]. Specifically, most of the research was performed in connection to Co [4,10–15], which promoted increased precipitation of carbides, successful transformation of RA into martensite and more homogenous and finer microstructure. In contrast, only few research papers discuss the influence of other carbide-forming alloying elements, such as Cr and W in combination with DCT [3–6]. Furthermore, most studies have been related to additional carbide type presence and basic mechanical properties, but not to the role of these elements on the DCT performance and on the microstructural changes during DCT. Within the last 15 years only Pellizzari [13] described the correlation of DCT performance to manufacturing type of HAFA. The work [13] showed that wrought HAFA have lower fracture toughness and higher wear resistance compared to PM HAFA when treated with DCT. Despite this, there is no concrete study performed on the simultaneous impact of both chemical composition and manufacturing type of HAFA on their modified microstructure and mechanical properties with DCT.

Furthermore, the testing of fatigue strength and fatigue limit in correlation with DCT is also limited to just a few studies on ferrous alloys [16–20], despite the fact that fatigue is the main determining factor, when improving the material performance, which defines the material life cycle. In addition, to our knowledge, the testing of fatigue properties of HAFA in correlation to DCT, was solely documented in our previous study by Jovičević-Klug and Podgornik [4]. Although there is a growing interest into HAFA due to high demand for improving mechanical properties such as toughness, strength and hardness, the DCT studies have been focused mainly on carbide formation and selected mechanical and wear properties, regardless of steel type [4,10–15], and with no deep correlation between steel type and chemistry. This indicates a lack of studies incorporating all of the following factors into one general research with emphasis on their interdependent impact on DCT effect. Additionally, no detailed research has been performed on the possible prediction of fatigue limit for HAFA in combination with DCT. Furthermore, no concrete models have been found in literature, when it comes to the specific HAFA of high-speed steels. The potential model could significantly improve the designing of such alloys, taking DCT into account for improving the fatigue properties. Additionally, the model could also be applied for material testing in industry, to reduce testing time and costs and provide a pragmatic description of fatigue properties based on the selected treatments and heat treatment parameters.

In this study, the correlation between different alloying content, presence of alloying elements and manufacturing type of HAFA to the effectiveness of deep cryogenic treatment is investigated. For a broad scope of research four different HAFA with two different manufacturing type (wrought (EN HS6-5-2 and EN HS6-5-2-5) and PM (EN HS6-5-3 and EN HS12-1-4)) were selected based on the content of alloying elements (W, Mo, V and Co). The goal of this research is to determine the impact of selected parameters on the microstructure of HAFA and selected mechanical properties, such as hardness, impact and fracture toughness as well as fatigue resistance. Within this research the findings are also explained in connection to the microstructural evolution and variation in regards to DCT. Additionally, a strain-life model is proposed to evaluate and predict the changes in fatigue properties based on the investigated factors (chemical composition, manufacturing type and DCT) that are directly related to the state of the microstructure and prior treatment (soft annealing) of the selected group of HAFA.

2. Experimental procedure

2.1. Material

Selected material for testing in this study were wrought HAFA, which were manufactured in wrought state (EN HS6-5-2, designated as W1, producer SIJ group, Ravne, Slovenia and EN HS6-5-2-5, designated as W2, producer Dörrenberg, Edelstahl GmbH, Engelskirchen, Germany) or by powder metallurgy (EN S6-5-3, designated as PM1, producer ERAsteel,

Hilden, Germany and EN HS18-0-1, designated as PM2, producer Boehler, Edelstahl GmbH, Engelskirchen, Germany). The alloys were supplied in a soft annealed state in the shape of peeled and rolled bars. The chemical composition of all four HAFA is provided in Table 1.

The selected heat treatment for each group is provided in Table 2. All samples were first austenitized and quenched in a single step in a horizontal vacuum furnace IPSEN VTTC-324R, Ipsen, Kleve, Germany with uniform high-pressure gas quenching using N_2 at the pressure of 5 bars (average quenching rate was approximately 7–8 °C s^{-1}). After quenching, the first specimen groups were conventionally heat-treated (CHT), comprising of double or triple tempering. The second groups were subjected to deep cryogenic treatment (DCT), performed immediately after quenching by gradual immersion of the samples in liquid nitrogen for 24 h (1 day) at −196 °C, followed by only a single tempering cycle, which is proven to be adequate enough due to nearly complete retained austenite transformation by DCT [13]. Heat treatment parameters are selected according to the steel producers' recommendations and previous findings of influence of selected heat treatment parameters on effectiveness of DCT in our prior publications [21,22].

Samples for mechanical and fatigue testing, manufactured from the received rods and subjected to heat treatment (Table 2) were prepared as CNPTB - Circumferentially Notched and fatigue Pre-cracked Tensile Bar specimens (for fracture toughness and hardness) [23] and CVN - Charpy V-notch (for impact toughness and fatigue). Samples for microstructure analysis and X-ray diffraction (XRD) were cut from CNPTB after testing. The sample preparation and sample testing follows the working procedure described in [24].

2.2. Methods

2.2.1. Phase and microstructural analysis

Phase analysis of all four ferrous alloys was performed with XRD. The XRD analysis was carried out on PANalytical 3040/60, Almelo, Netherlands and the XRD data was measured from 15° to 90° of 2θ angle. The phase identification was performed using COD database references and the volume fraction was determined using mass–volume relations extracted using combination of Rietveld refinement [25] and Toraya method [26]. Microstructural analysis was obtained by scanning electron microscope (SEM) (JEOL JSM-6500F, Jeol, Tokyo, Japan). Furthermore, two additional methods SEM-EDS (EDS is energy dispersive X-ray spectroscopy) and SEM-automated particle analysis (employed over the analyzing area of 400 × 400 μm^2) were used in order to obtain detailed information on microstructural changes induced by DCT in the selected ferrous alloys. To visualize the surface structures, Zeiss CrossBeam 550 (Zeiss, Oberkochen, Germany) dual beam FIB/SEM microscope was used. Cross-sections of the selected specimens were made by Ga^+ focused ion beam (FIB) machining, operating the beam at 30 keV energy and currents ranging from 3 nA to 100 pA. Energy dispersive spectroscopy (EDS) was used to measure the local chemical composition of microstructural features of the different samples using OctaneElite EDS detector (EDAX, Mahwah, NJ, USA).

Table 2 – Heat treatment parameters for selected wrought HAFA in designated groups, where CHT is conventionally heat-treated and DCT is deep cryogenic heat-treated.

Groups	Austenitizing (T (°C)/t (min))	DCT (T (°C)/t (h))	Tempering (T (°C)/t (h))
W1-CHT	1180/2	–	3x(620/1)
W1-DCT	1180/2	−196/24	1x(620/1)
W2-CHT	1160/2	–	3x(620/2)
W2-DCT	1160/2	−196/24	1x(620/2)
PM1-CHT	1050/2	–	3x(600/2)
PM1-DCT	1050/2	−196/24	1x(600/2)
PM2-CHT	1220/2	–	2x(600/2)
PM2-DCT	1220/2	−196/24	1x(600/2)

2.2.2. Mechanical testing and fatigue

2.2.2.1. Hardness (HRC). The hardness was measured by using Rockwell hardness method (HRC) according to the latest ISO standard SIST EN ISO 6508–1:2016. Testing was performed with Wilson Instruments B2000 machine, Bühler, Lake Bluffm IL, USA, carrying out at least three measurements on cylindrical parts of the CNPTB specimen (Fig. 1 a). The appropriate corrections of the measured results were employed depending on the diameter of the samples (Ø18 mm) according to the Annex C of the standard.

2.2.2.2. Fracture and impact toughness. To determine the fracture toughness of the material, the CNPTB specimens were used. The fatigue crack of ~0.5 mm was generated prior to the heat treatment by subjecting the sample to a single-point cyclic bending loading for several minutes. After heat treatment, the specimens (Fig. 1 a) were tested at room temperature by universal testing machine INSTRON 1255, Instron, Darmstadt, Germany with axial loading and strain rate of 0.001 s^{-1} until failure. The used evaluation procedure for fracture toughness is described in [23]. For each group, up to six specimens were tested and the average fracture toughness was reported in MPa$\sqrt{m}$. The impact toughness was determined by the Charpy impact test according to standard SIST EN ISO 148–1:2017. Testing was carried out on standard Charpy-V notch specimens (Fig. 1 b). Testing was conducted at room temperature with MLF, PSW 300 system with maximum

Table 1 – The chemical composition of selected HAFA in wt. %.

Ferrous alloy	C	W	Cr	Mo	V	Co	S	Mn	Fe
EN HS6-5-2 (W1)	0.90	6.00	4.00	4.70	1.70	–	0.002	0.28	base
EN HS6-5-2-5 (W2)	0.92	6.22	4.11	5.21	2.01	4.52	0.004	0.34	base
EN HS6-5-3 (PM1)	1.29	5.90	3.90	4.80	3.00	0.69	0.006	0.31	base
EN HS18-0-1 (PM2)	1.23	11.91	4.10	0.74	3.61	0.49	0.001	0.23	base

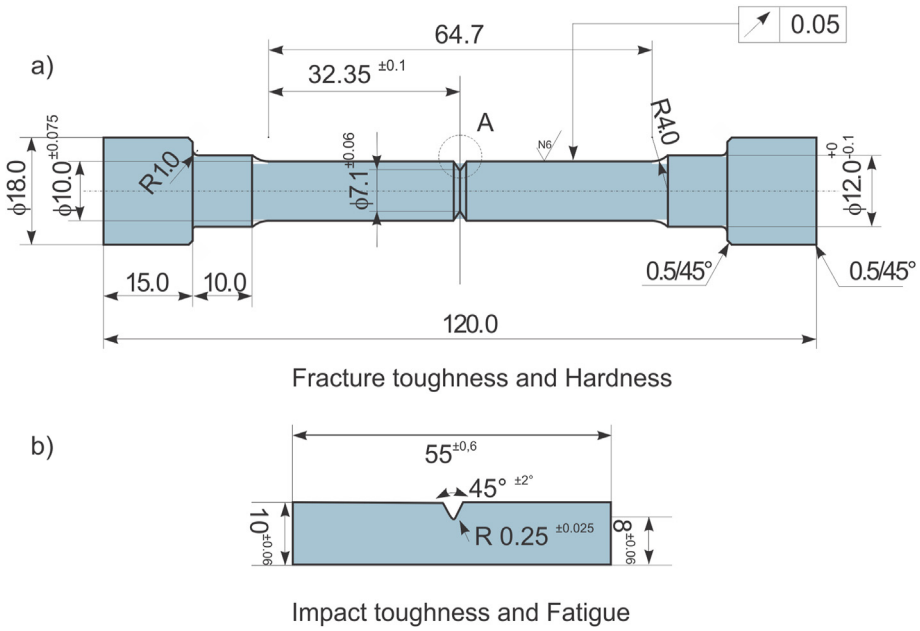

Fig. 1 – a) sample geometry for fracture toughness and hardness testing and b) Charpy-V notch test samples for impact toughness and fatigue testing.

energy capacity of 300 J. For each series three specimens were tested and the average impact toughness presented in absorbed energy (in J) was reported.

2.2.2.3. *Fatigue resistance*. Fatigue behavior of the investigated HAFA was determined under dynamic loading in bending mode using Rumul resonant fatigue testing machine Cracktronic, Russenberger AG, Neuhausen am Rheinfall, Switzerland, with an operating frequency of around 160 Hz. The fatigue (S/N) curves were obtained by performing room temperature fatigue tests on standard Charpy V-notched (CVN) samples (Fig. 1 b) and using constant amplitude bending stress between 220 MPa and 400 MPa, stress ratio R of 0.1 and a sinusoidal waveform. Sample failure criterion was set as a drop of inherent oscillation by more than 3%, where the fatigue cracks occurred in a depth of up to 3 mm.

2.2.3. *Strain-life behavior model*

The predication model for fatigue limit (failure model) is based on the combination of metallographic results of microstructure analysis and hardness measurement. The selected fatigue limit failure model is based on two Murukami equations (Eq. (1) and Eq. (2)) combined in one equation (Eq. (3)), as described by Murukami and Yamashita [27]. The Eq. (1), which was set and validated by Murukami [28], assumes that the stress intensity is identical for an inclusion and a crack under the same loading condition, for which the stress intensity factor (ΔK) at inclusion (in our case carbide) is expressed as follows. The ΔK depends on the stress value ($\Delta\sigma$), the inclusion area (carbides), factor $\alpha = 0.5$ is for inclusions present in the bulk of the sample and $\alpha = 0.65$ is for inclusions in contact directly with the surface.

$$\Delta K = \alpha \times \Delta\sigma \times \sqrt{\pi\sqrt{inclusion\ area}} \tag{1}$$

Murakami and Yamashita [27] (Eq. (2)) also assumed that short cracks behave differently compared to the long cracks in the material. The threshold value for cyclic crack propagation depends on the crack length itself. ΔK_{th} (in MPa$\sqrt{m}$) stands for threshold stress intensity failure range, which is correlated to the Vickers hardness (Hv) (units kgf/mm^2) and the effective inclusion area (carbides) (μm).

$$\Delta K_{th} = 0.00277 \times (H_V + 120) \times \left(\sqrt{inclusion\ area}\right)^{1/3} \tag{2}$$

From these two equations the derivation of the third equation (Eq. (3)) is possible. Eq. (3) states that the fatigue limit (σ_W) of selected metallic material results from the relationship between average inclusion (carbide) area and its hardness (H_v).

$$\sigma_W = \frac{1.56 \times (H_V + 120)}{\left(\sqrt{inclusion\ area}\right)^{\frac{1}{6}}} \tag{3}$$

To enable the transfer of the metallographic data to the inclusion area, parameter, Schumacher and Clausen [29], suggested use of an equivalent inclusion diameter, which is determined on the basis of the area of the largest inclusion. However, this model does not consider the different spatial arrangement of the carbides and carbide properties (hardness, the connection between carbide and (martensitic) matrix and carbide morphology). As such the model adapts the assumption of rounded particles, which gives a general description of a foreign particle weak point definition. In our approach we use the Murakami's expressions in relation to the different carbides found in the microstructures of selected HAFA, subjected to CHT and DCT.

The modeling of the data was performed in software Matlab, version R2019a, MathWorks, Natick, MA, USA, where the graphs were later altered by Origin, version 2021, OriginLab Corporation, Northampton, MA, USA.

3. Results

3.1. Phase and microstructural analysis

The phase analysis was investigated by XRD (Fig. 2) to determine the matrix, carbide type and carbide number in correlation to the chemical composition and manufacturing type. SEM particle analysis was additionally applied for determination of $M_{23}C_6$ fraction. The volumetric fraction for identified phases is presented in Fig. 2.

For all four HAFA (EN HS6-5-2 (W1), EN HS6-5-2-5 (W2), EN HS6-5-3 (PM1) and EN HS12-1-4 (PM2)), the matrix consists of lath martensite and <1 vol.% of retained austenite (RA). Three major types of carbides were detected, regardless of heat treatment, manufacturing type and chemical composition (concentration of W, Co and V): MC (V) (FCC), M_6C (Fe, Mo and W) (FCC) and $M_{23}C_6$ (Fe and Cr) (complex FCC). In addition to XRD, SEM-EDS also showed presence of individual highly decomposed M_2C carbides (HCP), which were more present for the wrought samples compared to the PM variants. In comparison the PM HAFA (PM1 and PM2) display increased precipitation, by roughly 300%, of MC carbides compared to wrought HAFA (W1–W2), regardless of the applied heat treatment procedure (CHT/DCT). In correlation to higher cobalt and tungsten concentrations, the W2 and PM2, with higher cobalt and tungsten concentration, respectively, show no significantly higher precipitation of $M_{23}C_6$ with DCT, compared to alloys with lower cobalt and tungsten values (W1 and PM1). However, the microstructure in all DCT samples is more homogenous compared to CHT samples.

The detailed carbide analysis (Table 3 and Fig. 3) was performed over several randomly selected areas with an area size of 400 × 400 μm2. The analysis showed that wrought steels subjected to DCT have on average a subordinate increase in carbides precipitation (25% in W1 (Fig. 3 a-b) and 12% in W2 (Fig. 3 c-d), accordingly) compared to PM steels, for which the carbide precipitation after DCT increased by 40% in PM1 (Fig. 3 e-f) and by 100% in PM2 (Fig. 3 g-h). Additionally, after DCT, the carbides displayed modified morphology (Table 3). For wrought samples, the carbides are rounder and more uniformly formed after DCT by roughly 15% for both wrought steel groups (W1 and W2 (Fig. 3 a-d)). Whereas, the observed roundness in both PM steel groups decreased after DCT by around 10% (PM 1 and PM2 (Fig. 3 e-h)). The carbides distribution in the samples was observed in correlation to nanocarbides (below 1 μm), for which the average nanocarbide size and average mean distance between carbides were discerned. The size of nanocarbides decreased with DCT treatment by roughly 40% for W1 (Fig. 3 b), 10% for W2 (Fig. 3 d), 5% for PM1 (Fig. 3 f) and 2% for PM2 (Fig. 3 h). In contrast, the average distance between carbides decreased for all four groups after DCT by roughly 10% for W1 (Fig. 3 b), 20% for W2 (Fig. 3 d), 50% for PM1 (Fig. 3 f) and 10% for PM2 (Fig. 3 h).

3.2. Hardness

The results of hardness measurements (Fig. 4 a) for wrought (W1, W2) and PM (PM1) HAFA alloys after DCT show slight increase in hardness ranging between 3 and 7% (W1-CHT ~58 HRC → W1-DCT ~60 HRC, W2-CHT ~53 HRC → W2-DCT ~57 HRC and PM1-CHT ~53 HRC → PM1-DCT ~56 HRC). However, for PM2 group hardness values for DCT and CHT are very similar (PM2-CHT ~62 HRC → PM2-DCT ~61 HRC), being within the Rockwell hardness measurement uncertainty. DCT has predominant positive effect on wrought HAFA in terms of increased hardness as compared to PM HAFA. From these results, it is clear that the manufacturing type has no direct influence on, whether DCT has a positive or a negative effect on hardness.

3.3. Fracture and impact toughness

Fig. 4b shows results of fracture toughness, where no clear trend of improvement in fracture toughness after application of DCT in relation to manufacturing type of HAFA can be observed. The increase in fracture toughness of about 15% is observed in W1 (W1-CHT ~12 MPa$\sqrt{m}$ → W1-DCT ~14 MPa$\sqrt{m}$) and PM2 (PM2-CHT ~13 MPa$\sqrt{m}$ → PM2-DCT ~15 MPa$\sqrt{m}$) groups. However, for W2 (W2-CHT ~12 MPa$\sqrt{m}$ → W2-DCT ~12 MPa$\sqrt{m}$) and PM1 (PM1-CHT ~15 MPa$\sqrt{m}$ → PM1-DCT ~12 MPa$\sqrt{m}$) no change or even decrease by 20% is observed, respectively.

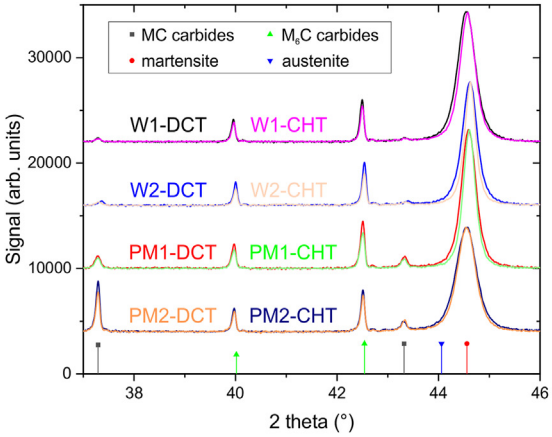

Material subgroup	Carbides			Matrix
	MC (V)	M_6C (W, Mo, Fe)	$M_{23}C_6$ (Fe, Cr)	
W1-CHT	1.8	6.7	2.5	89.1
W1-DCT	1.6	6.8	6.8	84.8
W2-CHT	2.8	7.1	3.4	86.7
W2-DCT	3.2	8.4	3.6	84.8
PM1-CHT	7.5	8.4	3.1	81.1
PM1-DCT	7.5	9.3	8.2	75.1
PM2-CHT	8	6.2	1.6	84.2
PM2-DCT	7.8	5.8	1.5	84.9

Fig. 2 – XRD results for all four groups of samples, where W stands for wrought HAFA, W1 (EN HS6-5-2), W2 (EN HS6-5-2-5), PM1 (EN HS6-5-3), PM2 (EN HS12-1-4) for both conventional (CHT) and deep cryogenic heat treatment (DCT).

Table 3 – The statistical analysis based on SEM particle analysis for carbides (above 1 μm) and nanocarbides (below 1 μm) for each steel (W1, W2, PM1 and PM2).

Group	Number of carbides per area (D/μm^2)	Roundness	Average nanocarbide size (nm)	Average distance between nanocarbides (nm)
W1-CHT	79.9	0.6 ± 0.26	540.2 ± 1.52	195.1 ± 0.35
W1-DCT	99.6	0.7 ± 0.22	236.5 ± 1.25	153.5 ± 0.67
W2-CHT	110.6	0.6 ± 0.26	162.1 ± 0.78	159.1 ± 0.17
W2-DCT	123.3	0.7 ± 0.25	149.1 ± 0.76	127.1 ± 0.18
PM1-CHT	115.8	0.7 ± 0.26	164.5 ± 2.04	88.0 ± 0.54
PM1-DCT	162.1	0.7 ± 0.21	157.9 ± 0.99	44.0 ± 0.28
PM2-CHT	97.0	0.8 ± 0.25	143.5 ± 0.67	143.3 ± 0.82
PM2-DCT	195.0	0.7 ± 0.28	141.5 ± 0.72	128.8 ± 0.93

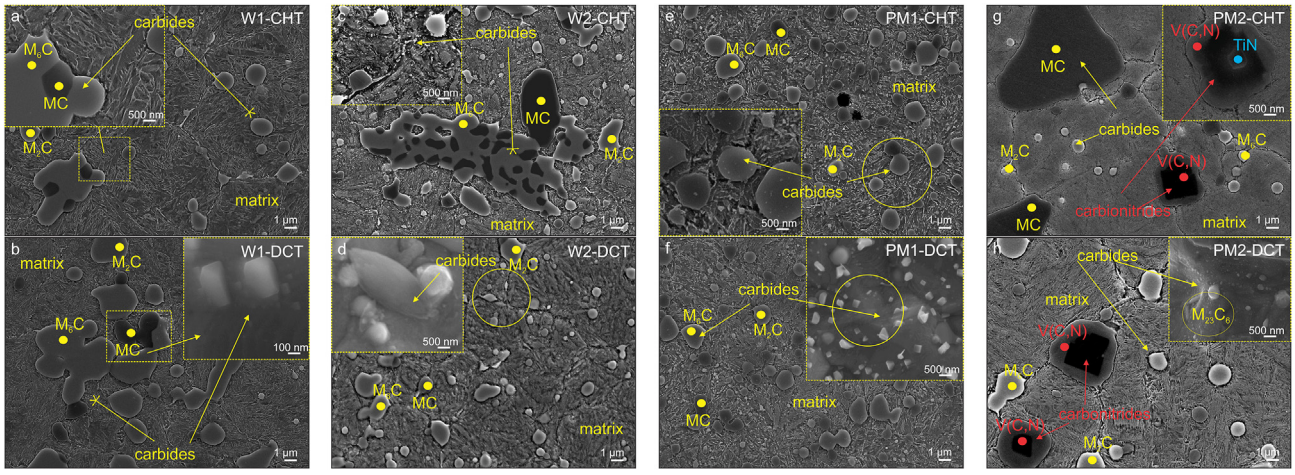

Fig. 3 – Microstructure of conventionally (W1-CHT (a), W2-CHT (c), PM1-CHT (e) and PM2-CHT (g)) and deep cryogenic heat-treated (W1-DCT (b), W2-DCT (d), PM1-DCT (f) and PM2-DCT (h)) samples.

Results of impact toughness measurement are provided in Fig. 4 c. The Charpy impact tests show no significant differences between all four investigated HAFA as well as in terms of applied heat treatment strategy (CHT or DCT). For all groups, results are between 3 and 4 J, indicating brittle nature selected HAFA with selected heat treatment parameters, which is common for such materials having hardness values above ~55 HRC. Nevertheless, some minor variations in the impact energy between CHT and DCT samples were observed for wrought samples, whereas for PM steels, no variation in impact energy was observed. This is associated to the presence of partially decomposed M_2C carbides, which have a strong impact on the stochastic fracture mechanics of wrought samples [5]. In all, the results indicate that impact toughness is not a relevant parameter for the identification of DCT induced changes for investigated HAFA.

3.4. *Fatigue resistance*

S–N curves for the investigated sample groups of HAFA are shown in Fig. 5. The results demonstrate a complexing relation of DCT effect on the fatigue resistance of selected HAFA. For the wrought steels the fatigue strength is in general only slightly altered by DCT. In the case of W1, the fatigue strength is increased, whereas for W2 it is decreased after DCT. In contrast, the fatigue limit is more impacted by DCT and in the opposite manner than the fatigue strength. The fatigue limit decreases by 10 MPa for W1 and increases by 30 MPa for W2 after DCT. For the PM steels the DCT influence is correlative for both fatigue strength and fatigue limit. For PM1, DCT is detrimental in terms of the fatigue properties, reducing the fatigue strength on average by 25 MPa and the fatigue limit by 20 MPa. Contrary, the PM2 fatigue properties are enhanced by DCT, increasing the fatigue strength on average by 10 MPa and the fatigue limit by 2.5 MPa. Proportional change in fatigue strength and fatigue limit for PM alloys and converse for wrought alloys can be associated to the finer microstructure of PM steels and to the significantly reduced presence of partially decomposed M_2C carbides (Fig. 3, Table 3). However, the fatigue results indicate additionally to the manufacturing type, the chemistry (alloying content, including Co, W, V and Mo) and microstructure of the different HAFA have a decisive role on the fatigue properties and their modification with DCT.

4. Discussion

4.1. *Microstructure*

In selected HAFA the concentration of alloying elements defines the type of precipitation of carbides and composition of depleted matrix (Fig. 3). The substantially higher content of W

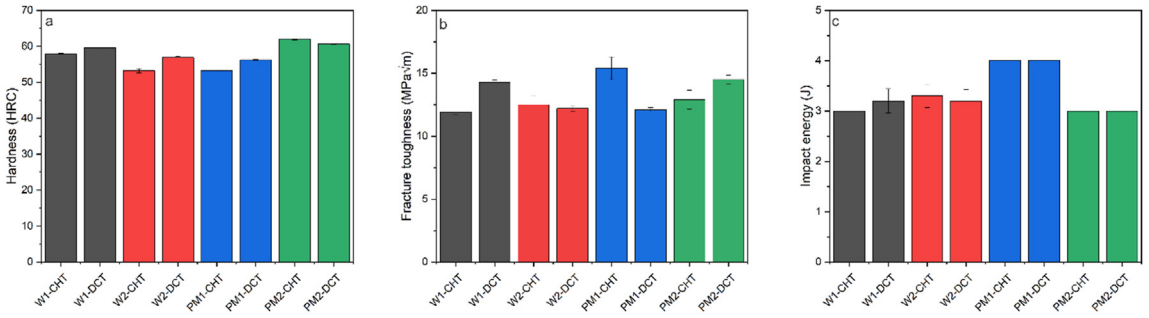

Fig. 4 – Mechanical properties of groups W1, W2, PM1 and PM2 for both heat treatments (CHT and DCT): a) hardness in HRC, b) fracture toughness in MPa$\sqrt{m}$ and c) impact toughness in J.

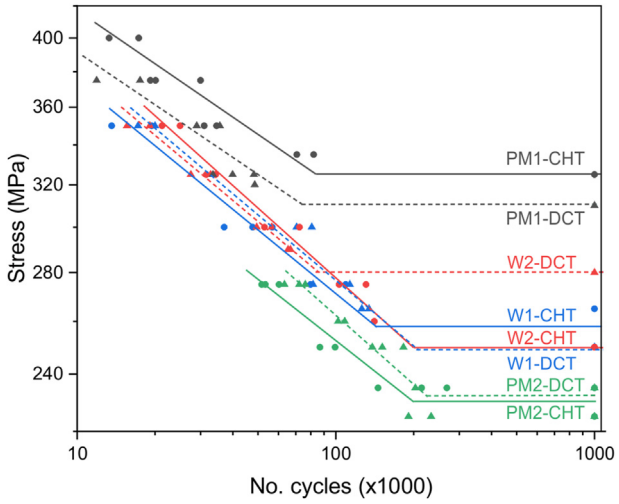

Fig. 5 – S–N curves of investigated HAFA W1, W2, PM1 and PM2, where CHT stands for conventional heat-treated and DCT for deep cryogenic heat-treated.

in PM2 alloy induced significantly higher W concentration in carbides and matrix, as compared to the other three sample groups (Table 4). Consequently, additional residual carbides such as M_2C ($(W, Mo, Fe)_2C$) and presence of some individual carbonitrides ($V(C_3, N)$-BCC) was observed in PM2 alloy (Fig. 3 h, Fig. 6). From literature [30], W is described to increases the homogeneity of the microstructure. However, no difference in this respect could be observed for the selected HAFA. Instead, DCT had the predominant effect on improving the homogeneity of the microstructure. This is achieved through the redistribution of alloying elements with DCT for all four HAFA, which increases the precipitation of carbides, especially smaller complex ones ($M_{23}C_6$), as shown also by our previous study Jovičević-Klug et al. [5]. Complementary to the redistribution also the transformation of retained austenite with DCT in contrast to decomposition through tempering also provides increased precipitation and reformation of carbides. Despite the different tempering times, the effective carbide precipitation is unaffected by the tempering times [31,32] and is instead determined by the enhanced carbide nucleation dictated by the modification of nucleation free energy and alloying elements agglomeration by DCT decomposition of retained austenite [5]. Additionally, the size of the martensitic laths in DCT samples is smaller by 10–35% as compared to CHT counterparts. With our previous research martensitic laths [4] are considered to be modified due to residual stress [33] and different path of austenite to martensite transformation, as well as carbide precipitation [5]. In addition, our previous study Jovičević-Klug and Podgornik [4] shows also that in HAFA the finer martensitic laths contribute to the local concentration gradient. In turn, this allows more homogeneous elemental distribution, due to shorter diffusional distances, based on the former austenitic grain boundaries. In connection to the influence of alloying elements, tungsten influences on both matrix and carbides, at which for HAFA with highest W concentration, the carbide precipitation is increased by 100% after DCT. This increased formation of hard an abrasion resistant W carbides [1] with DCT can increase hardness and wear resistance of the material. An additional interesting observation is that in PM2 steel with highest content of W and V, DCT also increases the formation of secondary vanadium carbonitrides (Fig. 6) by roughly 10%, which was observed for the first time for high-speed steels (for die cast steels a similar observation was claimed by Liu et al. [34]). The increased formation of vanadium carbonitrides can further explain enhanced properties of PM2 steel after DCT. The amplified presence of carbonitrides is confined more to the surfaces of the samples, indicating a relation to the direct contact of the surface with liquid nitrogen and could be possibly explained with the additional incorporation of nitrogen into the material's surface after DCT. The additional precipitation and growth of vanadium carbonitrides is also related to the diffusion coefficients of all three elements, especially V, as was shown by Maugis and Goune [35]. From the perspective of the carbide volumetric fraction change with DCT, there is a clear trend of reduced effect of DCT on $M_{23}C_6$ carbides for alloys with higher conjoined alloying content (W2 and PM2). This indicates that over-alloying results in preexisting presence of large amount of carbides that does not allow the possibility to further increase the volumetric fraction of carbides through precipitation of $M_{23}C_6$ carbides with DCT.

To understand the impact of individual chemical components on DCT effect of selected HAFA, thermodynamic modelling using CALPTHAD method was used by varying the alloying content of individual chemical elements. From the experimental results, W and Co are recognized as the main alloying elements that strongly influence the DCT effectiveness in terms of carbides precipitation. For this reason,

Table 4 – Average chemical composition of phases: lath martensite and precipitated carbides for both wrought (W1 and W2) and PM groups (PM1 and PM2), regardless of the heat treatment strategy, based on SEM-EDS results.

composition (wt. %)	C	W	Mo	Cr	V	Co	Fe
W1							
Matrix	0.5 ± 0.3	4.4 ± 0.5	3.9 ± 0.4	4.7 ± 0.2	1.1 ± 0.3	–	85.7 ± 1.3
MC	13.1 ± 0.8	18.3 ± 0.3	19.9 ± 0.5	4.1 ± 0.4	38.6 ± 0.7		6.2 ± 0.8
M_6C	2.8 ± 0.7	36.1 ± 0.6	24.8 ± 0.8	3.2 ± 0.1	2.9 ± 0.2		30.2 ± 0.4
M_2C*	9.2 ± 0.5	35.2 ± 0.5	21.9 ± 1.0	3.0 ± 0.2	2.6 ± 0.1		28.2 ± 0.3
W2							
Matrix	0.5 ± 0.3	4.5 ± 0.3	3.9 ± 0.7	4.7 ± 0.0	1.5 ± 0.2	5.5 ± 0.2	80.0 ± 1.0
MC	13.3 ± 2.9	17.1 ± 1.3	16.6 ± 0.5	4.7 ± 0.5	36.2 ± 0.4	5.1 ± 0.0	7.2 ± 2.3
M_6C	3.5 ± 0.4	33.4 ± 0.1	25.9 ± 0.9	3.1 ± 0.2	3.3 ± 0.3	2.5 ± 0.1	28.2 ± 0.0
M_2C*	10.0 ± 0.3	31.3 ± 0.1	24.5 ± 0.3	2.9 ± 0.2	2.6 ± 0.2	1.9 ± 0.3	26.7 ± 0.3
M_2C	9.1 ± 0.4	31.2 ± 0.2	35.3 ± 0.2	7.4 ± 0.2	11.1 ± 0.3	0.4 ± 0.0	5.5 ± 0.1
PM1							
Matrix	0.4 ± 0.3	2.6 ± 0.4	2.9 ± 0.0	4.3 ± 0.3	1.1 ± 0.3	2.1 ± 0.9	86.8 ± 1.2
MC	11.7 ± 0.3	16.8 ± 0.9	14.9 ± 0.6	4.6 ± 0.2	36.9 ± 0.8	4.1 ± 0.7	10.8 ± 0.8
M_6C	2.7 ± 0.4	35.2 ± 0.6	24.6 ± 0.5	3.1 ± 0.1	2.4 ± 0.2	3.2 ± 0.1	28.8 ± 1.5
M_2C*	8.3 ± 0.9	34.9 ± 0.6	23.8 ± 0.4	2.5 ± 0.0	2.6 ± 0.1	0	28.1 ± 0.8
PM2							
Matrix	0.4 ± 0.2	7.3 ± 0.3	1.5 ± 0.1	4.1 ± 0.1	1.5 ± 0.3	1.8 ± 0.2	83.4 ± 0.5
MC	11.9 ± 0.1	38.3 ± 0.3	1.7 ± 0.1	3.1 ± 0.2	40.6 ± 0.5	0	4.4 ± 0.3
M_6C	3.1 ± 0.1	62.1 ± 0.2	3.2 ± 0.2	2.3 ± 0.2	3.0 ± 0.2	0	26.3 ± 0.1
M_2C	9.3 ± 0.2	48.4 ± 0.3	2.3 ± 0.2	3.5 ± 0.1	19.0 ± 0.5	0	17.5 ± 0.5

Matrix-tetragonal martensite; MC–face centered cubic (FCC); M_6C-–face centered cubic (FCC); M_2C, M_2C* – hexagonal closed packed (HCP).

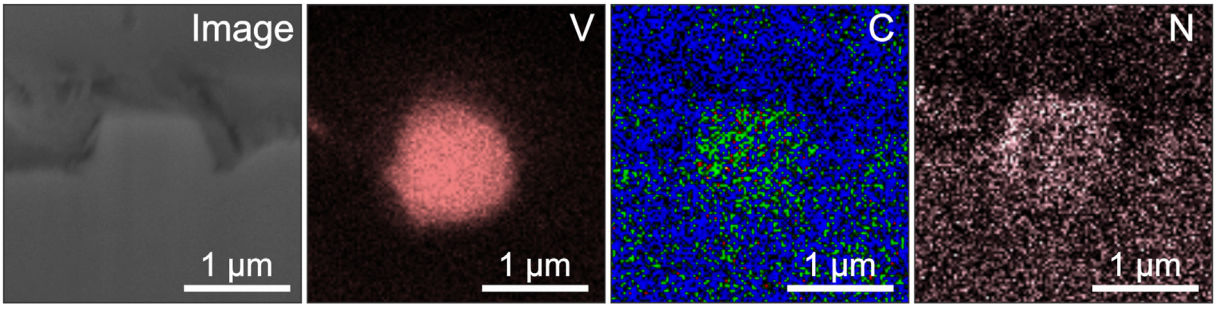

Fig. 6 – SEM image with accompanying energy dispersive X-ray spectroscopy maps of vanadium-based carbonitrides in steel PM2-DCT.

emphasis is given on these two elements. The modeling results (Fig. 7 a) indicate that increasing both W and Co content reduces the maximum achievable precipitation of $M_{23}C_6$ carbides as well as slows down the precipitation rate. W is considerably more effective in reducing the maximal achievable precipitation, whereas Co has a stronger influence on reducing the precipitation rate. This explains why PM2 generally displays the lowest precipitation volume. It also explains why the precipitation volume of $M_{23}C_6$ carbides increased only for W1 and PM1 after DCT due to their negligible Co content and medium W content. From the comparative simulated data for all investigated ferrous alloys (Fig. 7 b) it is clear that for W1 and PM1 alloys the precipitation is enhanced with DCT to the maximum achievable precipitation volume expected in theory. This evidently indicates that the alloying content not only influences the theoretical limit of precipitation, but also the extent of modified precipitation with DCT. Regardless of the manufacturing type, the high alloying content of W and Co results in negligible effect of DCT on total volume of precipitated carbides. It is proposed that the higher alloying with W and Co results in the initial formation of more stable primary carbides and lower chemical gradients, which in turn develop lower chemical gradients and available alloying elements for the formation of $M_{23}C_6$ carbides (see Fig. 7 a). In turn the additional influence of DCT is negligible, since the driving forces are not promoted by the additional shrinkage pressure effects (dislocation recombination and stress modification) that normally cause alloying elements agglomeration and redistribution. Despite this, the manufacturing type has a clear influence on the precipitation already in the CHT state. From modeled data it is clear that the wrought alloys had similar precipitation volume as expected in theory, whereas the PM alloys had effectively higher precipitation total volume as theoretically expected (Fig. 7 b). Surprisingly, despite the different experimental tempering times, both PM steels displayed a total volume of precipitates that equals to the volume achievable after around 9 h of tempering. This indicates that PM has a staggering influence

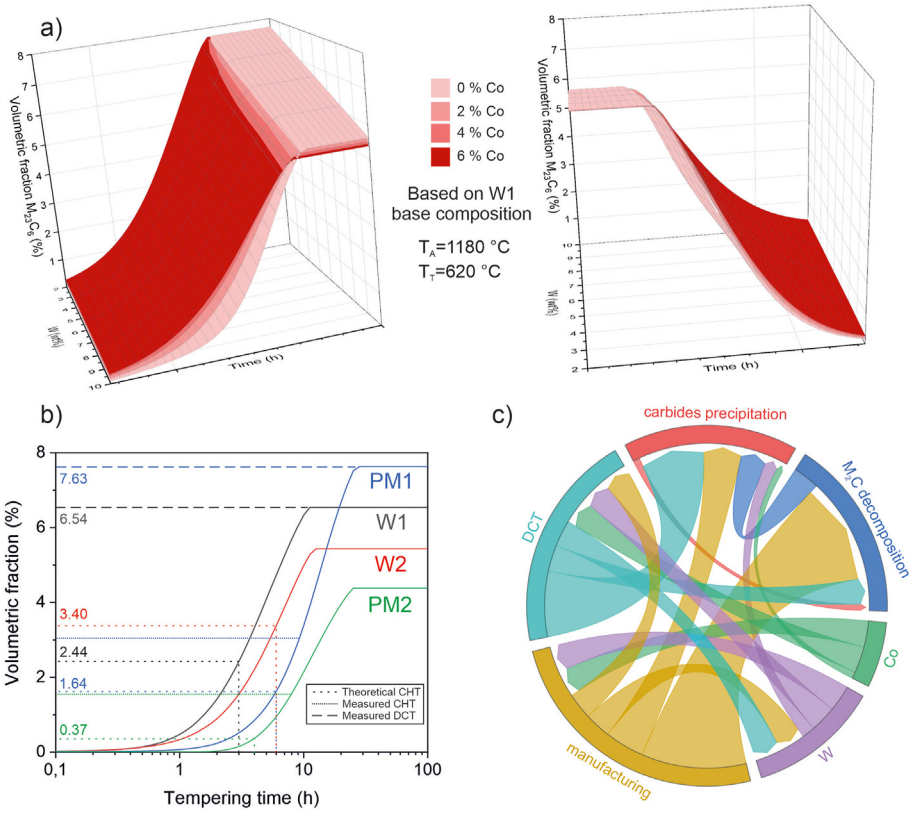

Fig. 7 – a) Modeled maps of $M_{23}C_6$ carbides precipitation with tempering time in dependency of varying W (axis) and Co content (color coding) presented from two different perspectives. The initial chemical composition is based on ferrous alloy W1 b) Modeled precipitation of $M_{23}C_6$ carbides for all investigated alloys with marked theoretical and measured volumetric fractions of $M_{23}C_6$ carbides. In the case of W1 and W2 the theoretical and measured CHT amounts are similar and not shown simultaneously. Additionally, for W2 and PM2 the DCT values are similar to the CHT values and are not shown for clarity of the data. c) Diagram depicting the relative interdependencies of the different parameters of investigated ferrous alloys.

on precipitation dynamics, which is also another factor that was observed to influence the DCT performance.

PM ferrous alloys have on average higher number of precipitated carbides, which are more homogeneously distributed, compared to wrought ferrous alloys, which was found in our investigation (Table 3) and also observed by Pellizzari [13]. Another observation related to the manufacturing type is correlated to the roundness of the precipitated carbides. For both wrought HAFA, precipitated carbides in DCT samples are rounder compared to precipitated carbides in CHT samples. In PM HAFA the carbides are more spherical already in CHT state compared to the carbides from wrought alloys. However, after application of DCT the carbides are less spherical compared to CHT samples of the PM HAFA. It is proposed that the difference in the morphological modification of the carbides stems from the more homogeneous microstructure and alloying composition of the PM steels. As a result, the growth kinetics of nanocarbides are not governed by concentration gradients, but instead driven by the lower energy states of individual facets. In turn this leads to a preferential growth of individual surfaces, which results in a reduced roundness of the carbides. Nevertheless, it also needs to be pointed out that DCT has been shown to induce additional formation of faceted carbides also for wrought steels, which is again associated with the more homogeneous distribution of alloying elements [5]. However, their faceted forms are less pronounced and more rounded as compared to PM samples from this study, which is considered to be related to the remaining residual local differences in alloying elements concentration. Another aspect of manufacturing process is also that wrought variants have on average larger precipitated nanocarbides with greater inter-carbides distance as compared to PM alloys, which confirms that DCT has greater effect on nanocarbides size in wrought alloys, compared to PM alloys.

Finally, an important perspective is related to the decomposition of M_2C carbides that are the primary carbides of the selected HAFA that form during their initial processing. The microstructural observations confirm that M_2C decomposition is enhanced by PM manufacturing and DCT. However, with higher alloying content of W, the decomposition is slowed down, which is clearly observed for PM2. On contrary, Co has a positive effect on M_2C decomposition as the resulting agglomerates are determined to be smaller at high Co content. This indicates a predetermined influence of the alloying content and related to the manufacturing process on the formation and decomposition of M_2C, which are key factors for the development of mechanical properties of HAFA (more discussion in following sections). The DCT affects the decomposition of M_2C carbides through the

activation of redistribution of alloying elements that also induces the increased precipitation of nanocarbides. This DCT effect has been thoroughly discussed in our previous publication [5].

From all of the microstructural observations and modelling data, it is clear that not only chemical composition of HAFA, but also manufacturing type (including vanadium carbonitrides that are formed during initial PM manufacturing) influence the DCT performance on microstructural development and thus alteration of material's properties (mechanical properties, wear and corrosion resistance). Altogether the findings display a complex arrangement of interconnected effects that have a defining influence on the microstructural evolution. In order to summarize the interdependencies in a concise manner, a dependency diagram depicting the relative cross-effects of individual aspects in a relative form is presented in Fig. 7 c. To note, the diagram shows a complex arrangement that hierarchically starts with the chemical composition and manufacturing from the initial metallurgical processing and austenitization. Afterward, DCT follows, which can once more influence the chemistry and microstructure development in the final tempering stage. To this point the carbide precipitation and M_2C decomposition are the final states that are also codependent on each other to a small degree.

4.2. *Hardness*

Hardness results confirm, that higher W content in HAFA initiates higher hardness. Tungsten's high content in both matrix and carbides shows double hardening effect, one by solid solution hardening and the other by increasing the hardness of the M_6C and M_2C carbides by replacing Mo. Hardness results also show more pronounced effect of DCT on hardness in wrought HAFA as compared to PM ones. The possible explanation for this is the reduced effect of solid solution hardening of the martensitic matrix due to the higher number of nanocarbides and overall increased volumetric fraction of carbides, as compared to wrought HAFA. Furthermore, in wrought as well as in PM1 samples, the number and volumetric fraction of precipitated carbides is increased after DCT (Fig. 2). However, in PM2 alloy, showing decreased hardness after DCT, can be related to the unaltered volumetric fraction of carbides after DCT, albeit increasing total number of nanocarbides (Fig. 2) and reduced solid solution hardening. This suggests, that W and volumetric fraction of W-nanocarbides play a crucial role in the DCT effectiveness on hardness increase in HAFA. The higher content of W generally, reduces the $M_{23}C_6$ formation, regardless of the HAFA and manufacturing type (PM/wrought), as shown in Fig. 7 a (example for HAFA-W1). With this, the achieved precipitation effect with DCT is negligible in comparison to CHT, since CHT already induces $M_{23}C_6$ precipitation close to the theoretically achievable volume fraction, see Fig. 7 b. Additionally, with higher W the higher hardening of M_2C and M_6C forms, as well as high solid solution strengthening of the matrix. Together both of these effect result in high overall hardness of HAFA, which can be only marginally modified with DCT, through additional carbide precipitation and local chemical modification.

4.3. *Impact and fracture toughness*

The toughness measurements do not show a clear trend for DCT influence depending on the alloy manufacturing type and alloy composition. However, certain differences between different HAFA were observed. As expected, for PM alloys increase in hardness obtained with DCT is accompanied with drop in fracture toughness and vice versa (Fig. 4), being mainly related to the change in matrix hardness. However, in the case of wrought alloys, DCT increases alloy hardness without reducing (W2) or even increasing (W1) toughness. The simultaneous increase for W1 alloy can be related to the combined effect of more spherical shape, higher density and much smaller size of nanocarbides after DCT, providing a microstructure, which does not allow fast bridging and crack propagation through the nanocarbides thus resulting in increased fracture toughness as compared to CHT counterpart. For the W2 alloy, similar fracture toughness after DCT and CHT is measured, despite the increased hardness after DCT, resulting from the high alloying with Co, which serves as a moderator of the diffusion mobility of W [36]. In turn, this allows increased decomposition of M_2C carbides and redistribution of W in the material that leads to toughness stabilization [37]. This is supported by the considerably higher amount of carbides for W2 compared to W1 (Table 3) and similar W content in the matrix (Table 4), despite both having the same amount of carbide-forming alloying elements (W, Mo, Cr, V). In the case of PM1 steel considerable drop in fracture toughness after DCT is also related to the increased precipitation and volume fraction of carbides. In this regards it should be noted that based on the similar chemical composition such relation would be expected also for the wrought alloy W1. However, the significantly higher presence of M_2C carbides for wrought alloy and more rounded form of nanocarbides after DCT are the deciding reason for improved fracture toughness in the wrought alloy as compared to PM one. In relation to impact toughness, the refined martensitic lath size and chemical depletion of alloying elements after DCT play an additional general role regardless of the alloying and manufacturing of HAFA. Both of these features result in a stronger yet more flexible matrix that translates to additional improvement of the impact toughness [22]. However, as mentioned the negative impact resulting from carbide precipitation needs to be also considered, when evaluating the overall impact of DCT on impact toughness.

4.4. *Fatigue resistance*

Fatigue results indicate that additionally to the major alloying elements (Co, Mo and W), V may also play a role on fatigue properties of the investigated HAFA and the effect of DCT. Different amount of V does not necessarily result in the corresponding amount of vanadium carbides. As a result, the increased amount of vanadium has to be compensated by the incorporation of V in the matrix in the form of a solid solution or incorporated into the complex partially decomposed M_2C carbides and nanometer-sized precipitated carbides (below detection limit of XRD and SEM). Regardless of the mechanism, the vanadium-enriched matrix is thus hardened, which in turn increases the strength and fatigue properties of the

material. As shown for medium alloyed steels [38] and the range of dissolved V found in the investigated alloys, increased alloying with V generally results in improved fatigue strength and fatigue ratio. In the case of this study, it is believed that the increased fatigue limit and strength for W2 and PM2 obtained by DCT is associated to the previously explained effect of increased strength of the matrix. For the W2 steel the fatigue strength is relatively unchanged after DCT, which is a result of the high Co presence that allows improved W mobility as discussed in section 4.4, thus reducing the strength and counteracting the effect of V modification with DCT.

The lowest overall fatigue properties of PM2 alloy in both CHT and DCT state, are due to its low Mo content and the lack of alloying of the M_6C carbides of the form of Fe_3W_3C with Mo, which would normally result in a complex carbide form of $Fe_3(W,Mo)_3C$. With higher content of Mo, the carbides are more enriched with Mo, which display higher ductility and resistance to cracking. In turn, the more ductile carbides result in increased resistance of the material to crack propagation, effectively leading to an increase of the fatigue limit. A similar observation with regards to Mo effect on such types of HAFA has been provided by Sohar et al. [39]. In retrospect, the PM1 steel exhibits the highest fatigue properties of all selected steels, due to its high V and Mo presence coupled together with the refined microstructure from the PM process that results in higher carbide density, compared to the two wrought steels W1 and W2. Negative effect of DCT on fatigue properties of PM1 steel is due to the significantly increased volumetric fraction and density of $M_{23}C_6$ carbides after DCT. The carbides act as defects and due to their faceted morphology act as crack initiation sites and can easily form crack bridging due to their short inter-carbides average distance, thus resulting in lower fatigue limit and strength. Similarly, this effect is also present in W1, but with the exception of the fatigue strength, as the increased decomposition of M_2C carbides with DCT reduces the weak-point crack formation [5,22]. For exactly the same reason coupled with the increased strength of the matrix due to higher V, the W2 displays such a significant improvement in the fatigue limit with DCT.

4.5. *Strain-life behavior model*

With the above discussed points and microstructure conclusions, the varying DCT effect on fatigue properties can be explained and further evaluated through a strain-life behavior model. The first adaption of Murakami's equations is to describe the carbides as inclusions that represent the most effective weak points of each investigated ferrous alloy. In our case, the large elongated rounded-shaped M_2C carbides are considered to be the most critical weak points due to their low strength and large form. A proof of their highest mechanical instability is also observed by their cracking during metallographic sample preparation (see Supplementary material 1). However, the estimation of their effective size is not straightforward. These carbides decompose during the heat treatment of the material from their M_2C structure to MC and M_6C carbides that remain in an agglomerated form as seen in Fig. 3 c. The decomposition is not ideal and often leads to partial decomposition of the carbides [5]. As such, the size needs to be assumed based on the decomposition fraction and on the size of resulting agglomerates (see Supplementary material 1). Without accommodating these features, the Murakami model underestimates the fatigue limit (example given in Fig. 8 a-b, full data presented in Supplementary material 2 and Supplementary material 3). Nevertheless, the Murakami predictions are still closer towards the measured values in comparison to the empirical model from Bandara

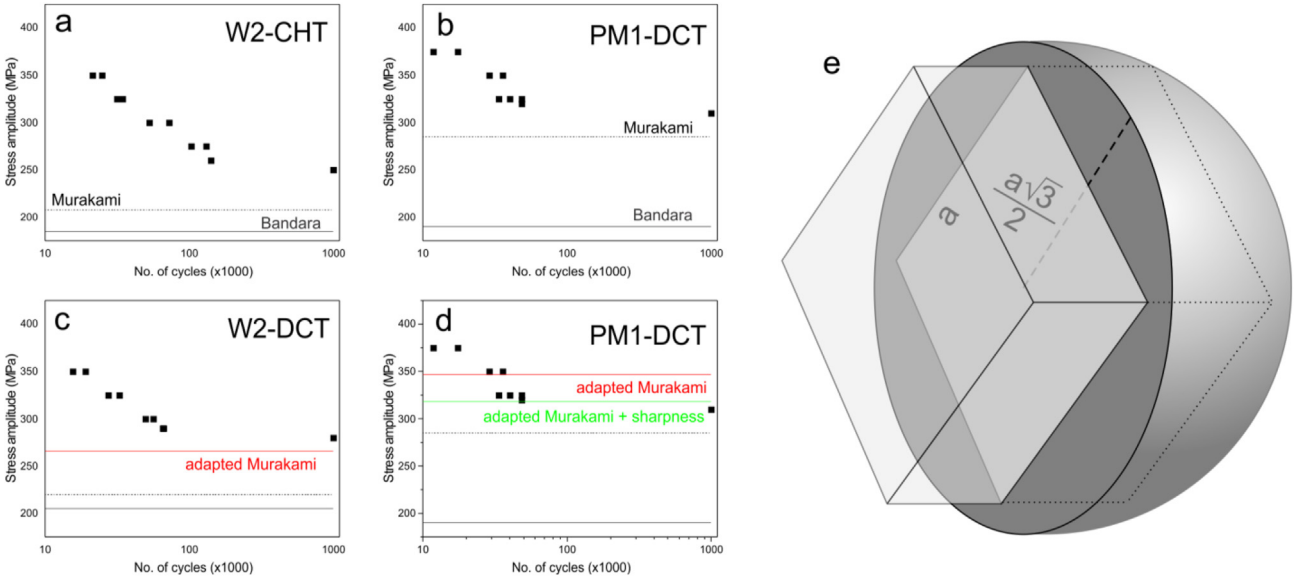

Fig. 8 – Exemplar fatigue data of selected ferrous alloys with already known models (a and b) and with the adapted Murakami models (c and d). e) A sketch of the idealized cubic carbide form and its effective stress field represented by a circumscribed sphere. The basic parameters of both bodies is provided in the sketch, at which *a* represents the side length of the cube.

[40], that is commonly used for ferrous alloys for tooling industry applications (comparison in Fig. 8 a-b).

In order to correct the shortcomings of the Murakami model, the following assumptions based on the microstructural analysis are considered. For W1, W2 and PM1 alloys very strong decomposition takes place, with the residual fraction of the M_2C carbides being in the range of 10% or lower, thus making their effective size only 10% of the agglomerates size. In the case of PM2 the decomposition is considerably slower due to the high W content, propagating by only about 60% of the total volume of the M_2C carbides (determined from frequency and size of carbides). This means that only 40% of the agglomerates size is effective as weak points. Additionally, for PM1 alloy no large agglomerates were found due to the PM manufacturing and its alloying content. In this case, the largest nanosized precipitated $M_{23}C_6$ carbides are considered as the weakest points due to their high occurrence and low average hardness compared to the other carbides of selected ferrous alloys [21]. With the adjustments of the effective weak point size (decomposition factor), the adapted Murakami model describes well the different fatigue limits for selected ferrous alloys (see red line in Supplementary material 2 and Supplementary material 3). From Fig. 8 c-d the adapted Murakami model (red line) is shown to work well for the CHT variants, while it overestimates the fatigue limit values for W1 and PM1.

Overestimation for DCT is considered to originate from the modification of the nanocarbides precipitation with DCT that also results in their morphological change. In our specific case, the nanosized carbides after DCT are cuboidal and thus have a stronger impact on the crack propagation with their much notch-like edges. In order to incorporate this effect, Murakami's Eq. (3) has been adapted. Our approach uses the definition of stress concentration determination for voids in materials defined by Kirsher [41] and Ingles [42]. In our specific case the edges of the carbides can be represented as small notches, which effectively induce larger stress concentrations. By starting with stress concentration (K_I) definition of Ingles (Eq. (4)):

$$K_I = 1 + 2\sqrt{\frac{l}{r}} \tag{4}$$

This can be related to the half-length of the carbides (l) with the radius (r) of the inscribed radius of the edge. For the nanosized cuboidal carbides the inscribed radius of the sphere should be theoretically close to 1 atom, giving nearly infinite K_I. However, effectively the stress field of interest is not at the tip of the edges, but rather at the distance where the neighboring edges of the carbides effectively act equally on the stress state of the surrounding material. This projects a rounded shape of the effective stress field that is described by Kirsher and is implied in the Murakami's Eq. (3). The derivation of the volume expansion follows a simple geometric extraction of a circumscribed sphere, which is an idealized effective stress field [42] of an ideal cubic carbide (sketch provided in Fig. 8 e). As such, the effective volume of the carbides (correlated through average cross-section of the weak point) is then extended by a factor of 2.72 (volume of sphere divided by volume of cube). With this factor (denoted as nanocarbides sharpness factor) the effective area of the nanocarbides of cuboidal form can be corrected.

The added factor for W1-DCT and PM2-DCT samples correlates well with the measured fatigue. Note that for W2-DCT and PM2-DCT no cuboidal nanocarbides were found (nanocarbides sharpness factor = 1), which is a result of the different available thermodynamic evolution of the carbides with DCT [5].

With the final correction factor, the fatigue properties can be well described for both CHT and DCT variants of the investigated ferrous alloys. The finalized modified Murakami's Eq. (5) is provided below:

$$\sigma_W = \frac{1.56 \times (H_V + 120)}{\left(\sqrt{\textit{average cross section of weak point} \cdot \textit{decomposition factor} \cdot \textit{nanocarbides sharpness factor}}\right)^{\frac{1}{6}}} \tag{5}$$

Although the equation holds very well for the investigated HAFA and specific heat treatment states, a wider application of this model adaptation needs to be further investigated by using a larger assortment of HAFA ferrous alloys and tested with different heat treatment conditions and parameters.

5. Conclusions

The effectiveness of deep cryogenic treatment (DCT) was evaluated based on the alloying content and manufacturing type of four high-alloyed ferrous alloys (HAFA). Overall, DCT has greater effect on wrought HAFA than PM HAFA.

- DCT has effect on precipitation of carbides and nanocarbides, where size, roundness, average distance between carbides/nanocarbides, phase and matrix (martensitic) laths are modified. The stronger effect of DCT on nanocarbides and their increased precipitation is observed in wrought HAFA, compared to PM HAFA. However, an important role on mechanical properties also have W-rich nanocarbides and vanadium carbonitrides.
- The chemical composition has a dominant role on the microstructural evolution set by the manufacturing type and on the DCT effectiveness on the microstructural evolution and carbide precipitation. W and Co in higher quantities generally retard the increase in volumetric fraction of precipitated carbides and thus block the precipitates volume increase with DCT. However, Co supports increased number of precipitates.
- Hardness is strongly influenced by tungsten and the improvement of hardness after application of DCT is

preferential for lower W-concentrations, which is strongly associated with W-rich nanocarbides.
- DCT effect on the toughness and fatigue properties is correlated to W and Co content and partly to manufacturing type, which is associated with the carbide's distribution and density.
- Strain-life modelling confirmed the observed trend in fatigue properties related to the microstructural development with different manufacturing type and presence of DCT. With the basic Murakami model with added correction factors (M_2C carbides decomposition and nanocarbides sharpness), extracted from the modified microstructures, the fatigue limit of all investigated samples can be determined with high correlation to the measured data. The model provides the first basis for a simplistic determination of the fatigue limit of HAFA with and without the additional effect of DCT.

Data availability

The raw/processed data required to reproduce these findings cannot be shared at this time as the data also forms part of an ongoing study.

CRediT authorship contribution statement

P.J.-K.: Conceptualization, Methodology, Investigation, Visualization, Writing-Original Draft, Writing-editing and review.

A.Z.G.: Methodology, Writing-Original Draft, Writing-editing and review.

M.J.-K.: Methodology, Investigation, Visualization, Resources, Writing-Original Draft, Writing-editing and review.

B.Š.B.: Methodology, Writing-Original Draft, Writing-editing and review.

A.L: Methodology, Writing-Original Draft, Writing-editing and review.

B.P.: Conceptualization, Supervision, Resources, Writing-editing and review.

All authors have read and agreed to the published version of the manuscript.

Funding

This work was supported by Slovenian Research Agency (ARRS), Ljubljana, Slovenia [No. P2-0050 & No. J2-9211].

Declaration of Competing Interest

The authors declare that they have no known competing financial interests or personal relationships that could have appeared to influence the work reported in this paper.

Acknowledgement

Acknowledgement goes to collogues B. Zvonar (IMT) for the help with heat treatments, N. Lipovšek (IMT) and T. Kranjec (IMT) for the help in the metallographic lab, G. Puš (IMT) for the help in mechanical lab and T. Sever (IMT) as SEM operator.

Appendix A. Supplementary data

Supplementary data to this article can be found online at https://doi.org/10.1016/j.jmrt.2022.04.025.

REFERENCES

[1] Totten GEPD. Steel heat treatment. Met Technol 2007:1–1558. https://doi.org/10.1201/NOF0849384523.ch6.
[2] Jovičević-Klug P, Podgornik B. Review on the effect of deep cryogenic treatment of metallic materials in automotive applications. Metals 2020;10:434. https://doi.org/10.3390/met10040434.
[3] Pellizzari M, Molinari A, Girardini L, Maldarelli L. Deep cryogenic treatment of AISI M2 high-speed steel. Int J Microstruct Mater Prop 2008;3:383–90. https://doi.org/10.1504/IJMMP.2008.018742.
[4] Jovičević-Klug P, Podgornik B. Comparative study of conventional and deep cryogenic treatment of AISI M3:2 (EN 1.3395) high-speed steel. J Mater Res Technol 2020;9:13118–27. https://doi.org/10.1016/j.jmrt.2020.09.071.
[5] Jovičević-Klug P, Jovičević-Klug M, Podgornik B. Effectiveness of deep cryogenic treatment on carbide precipitation. J Mater Res Technol 2020;9:13014–26. https://doi.org/10.1016/j.jmrt.2020.09.063.
[6] Pellizzari M, Caliskanoglu D, Fernández A, Barbero JI, Pena B, Uemit T, et al. Influence of different deep cryogenic treatment routes on the properties of high speed steel. HTM J Heat Treat Mater. 2012;67:111–7.
[7] Xu G, Huang P, Wei Z, FAng Z, Zu G. Microstructural variations and mechanical properties of deep cryogenic treated AISI M35 high-speed steel tempered at various temperatures. J Mater Res Technol 2022:118159. https://doi.org/10.1016/j.jmrt.2022.02.083.
[8] Zhou L, Min N, Li H, Wu X, Wu X. Nanoscratch and internal friction investigations of deep cryogenic treated M2 high-speed steel. Https://Doi.Org/10.1080/25787616.2020.1748340. 1. 2020. p. 109–14. https://doi.org/10.1080/25787616.2020.1748340.
[9] Li S, Xiao M, Ye G, Zhao K, Yang M. Effects of deep cryogenic treatment on microstructural evolution and alloy phases precipitation of a new low carbon martensitic stainless bearing steel during aging. Mater Sci Eng 2018;732:167–77. https://doi.org/10.1016/j.msea.2018.07.012.
[10] da Silva FJ, Franco SD, Machado ÁR, Ezugwu EO, Souza AM. Performance of cryogenically treated HSS tools. Wear 2006;261:674–85. https://doi.org/10.1016/j.wear.2006.01.017.
[11] Candane D. Effect of cryogenic treatment on microstructure and wear characteristics of AISI M35 HSS. Int J Mater Sci Appl 2013;2:60. https://doi.org/10.11648/j.ijmsa.20130202.14.
[12] Leskovšek V, Podgornik B. Simultaneous ion nitriding and tempering after deep cryogenic treatment of PM S390MC HSS. Int Heat Treat Surf Eng 2013;7:115–9. https://doi.org/10.1179/1749514813Z.00000000066.
[13] Pellizzari M. Influence of deep cryogenic treatment on the properties of conventional and PM high speed steels. Metall. Ital. 2008;100:17–22.
[14] C.L. Gogte, D.R. Peshwe, R.K. Paretkar, Influence of cobalt on the cryogenically treated W-Mo-V high speed steel, in: Adv.

Cryog. Eng., Spokane, WA, USA, n.d.: pp. 1175–1182. https://doi.org/10.1063/1.4707039.
[15] Dhokey NB, Hake A, Kadu S, Bhoskar I, Dey GK. Influence of cryoprocessing on mechanism of carbide development in cobalt-bearing high-speed steel (M35). Metall Mater Trans A Phys Metall Mater Sci 2014;45:1508–16. https://doi.org/10.1007/s11661-013-2067-2.
[16] Baldissera P, Delprete C. Effects of deep cryogenic treatment on static mechanical properties of 18NiCrMo5 carburized steel. Mater Des 2009;30:1435–40. https://doi.org/10.1016/j.matdes.2008.08.015.
[17] Dumasia CA, Kulkarni VA. Effect of cryogenic treatment on EN8 steel used for press tool. Glob J Engieering Sci Res Manag 2017;4:39–54. https://doi.org/10.5281/zenodo.841202.
[18] Gao W, Wang X, Chen J, Ban C, Cui J, Lu Z. Influence of deep cryogenic treatment on microstructure and properties of 7A99 ultra-high strength aluminum alloy. Met 2019;9:631. https://doi.org/10.3390/MET9060631.
[19] Myeong TH, Yamabayashi Y, Shimojo M, Higo Y. A new life extension method for high cycle fatigue using micro-martensitic transformation in an austenitic stainless steel. Int J Fatig 1997;19:69–73. https://doi.org/10.1016/s0142-1123(97)00060-1.
[20] Baldissera P, Delprete C. Deep cryogenic treatment: effects on mechanical properties of AISI 302 stainless steel and 18NiCrMo5 carburized steel. Key Eng Mater 2009;417–418:793–6. https://doi.org/10.4028/www.scientific.net/KEM.417-418.793.
[21] Jovičević-Klug P, Sedlaček M, Jovičević-Klug M, Podgornik B. Effect of deep cryogenic treatment on corrosion properties of various high-speed steels. Materials 2021;14:1–16. https://doi.org/10.3390/met11010014.
[22] Jovičević-Klug P, Puš G, Jovičević-Klug M, Žužek B, Podgornik B. Influence of heat treatment parameters on effectiveness of deep cryogenic treatment on properties of high-speed steels. Mater Sci Eng 2022;829:142157. https://doi.org/10.1016/j.msea.2021.142157.
[23] Podgornik B, Žužek B, Leskovšek V. Experimental evaluation of tool steel fracture toughness using circumferentially notched and precracked tension bar specimen. Mater Perform Charact 2014;3:87–103.
[24] Jovičević-Klug P, Puš G, Jovičević-Klug M, Žužek B, Podgornik B. Effect of deep cryogenic treatment on mechanical properties of high-speed steels. Mater Sci Eng 2022;829:142157.
[25] Rietveld HM. A profile refinement method for nuclear and magnetic structures. J Appl Crystallogr 1969;2:65–71. https://doi.org/10.1107/s0021889869006558.
[26] Toraya H. A new method for quantitative phase analysis using X-ray powder diffraction: direct derivation of weight fractions from observed integrated intensities and chemical compositions of individual phases. J Appl Crystallogr 2016;49:1508–16. https://doi.org/10.1107/S1600576716010451.
[27] Murakami Y, Yamashita Y. Prediction of life and scatter of fatigue failure originated at nonmetallic inclusions. Procedia Eng 2014;74:6–11. https://doi.org/10.1016/J.PROENG.2014.06.214.
[28] Murakami Yukitaka. Metal fatigue: effects of small defects adn nonmetallic inclusions. 1st ed. Amsterdam, Netherlands: Elsevier Science; 2002.
[29] Schumacher J, Clausen B. Calculation of the fatigue limit of high-strength steel specimens at different loading conditions based on inclusion sizes. Steel Res Int 2021. https://doi.org/10.1002/srin.202100252. 2100252.
[30] Lv Y, Sun Y, Zhao J, Yu G, Shen J, Hu S. Effect of tungsten on microstructure and properties of high chromium cast iron. Mater Des 2012;39:303–8. https://doi.org/10.1016/J.MATDES.2012.02.048.
[31] Darwin JD, Mohan Lal D, Nagarajan G. Optimization of cryogenic treatment to maximize the wear resistance of 18% Cr martensitic stainless steel by Taguchi method. J Mater Process Technol 2008;195:241–7. https://doi.org/10.1016/j.jmatprotec.2007.05.005.
[32] Jovičević-Klug P, Jovičević-Klug M, Sever T, Feizpour D, Podgornik B. Impact of steel type, composition and heat treatment parameters on effectiveness of deep cryogenic treatment. J Mater Res Technol in progres 2021:1–23.
[33] Jovicevic-Klug M, Jovicevic-Klug P, McCord J, Podgornik B. Investigation of microstructural attributes of steel surfaces through magneto-optical Kerr effect. J Mater Res Technol 2021;11:1245–59. https://doi.org/10.1016/J.JMRT.2021.01.106.
[34] Liu S, Wu X, Shi L, Wu Y, Qu W. Influence of cryogenic treatment on microstructure and properties improvement of die steel. J Mater Sci Chem Eng 2015;3:37–46. https://doi.org/10.4236/MSCE.2015.39005.
[35] Maugis P, Gouné M. Kinetics of vanadium carbonitride precipitation in steel: a computer model. Acta Mater 2005;53:3359–67. https://doi.org/10.1016/j.actamat.2005.03.036.
[36] Gulyaev AP, Kupalova IK. Effect of cobalt on the structure and properties of high-speed steels. Met Sci Heat Treat 1970;12:666–71. https://doi.org/10.1007/BF00654791. 1971 128.
[37] Garrison WM. Cobalt and the toughness of steel. Mater Sci Forum 2012;710:3–10. https://doi.org/10.4028/WWW.SCIENTIFIC.NET/MSF.710.3.
[38] Hui W, Chen S, Zhang Y, Shao C, Dong H. Effect of vanadium on the high-cycle fatigue fracture properties of medium-carbon microalloyed steel for fracture splitting connecting rod. Mater Des 2015;66:227–34. https://doi.org/10.1016/J.MATDES.2014.10.064.
[39] Sohar CR, Betzwar-Kotas A, Gierl C, Weiss B, Danninger H. Fatigue behaviour of M2 and M42 high speed steel up to the gigacycle regime. Kov. Mater. 2009;47:147–58.
[40] Bandara CS, Siriwardane SC, Dissanayake UI, Dissanayake R. Developing a full range S–N curve and estimating cumulative fatigue damage of steel elements. Comput Mater Sci PA 2015:96–101. https://doi.org/10.1016/J.COMMATSCI.2014.09.009.
[41] Kirsch EG. Die Theorie der Elastizität und die Bedürfnisse der Festigkeitslehre. Zeitschrift Des Vereines Dtsch. Ingenieure. 1898;42:797–807.
[42] Inglis CE. Stresses in plates due to the presence of cracks and sharp corners. Trans Inst Nav Archit 1913;55:219–41.